HHS Public Access

Author manuscript

J Control Release. Author manuscript; available in PMC 2019 January 09.

Published in final edited form as:

J Control Release. 2016 April 10; 227: 38–44. doi:10.1016/j.jconrel.2016.02.016.

Analyzing Spatiotemporal Distribution of Uniquely Fluorescent Nanoparticles in Xenograft Tumors

Darren L. Stirland[a], **Yu Matsumoto**[b,c], **Kazuko Toh**[b], **Kazunori Kataoka**[d], and **You Han Bae**[e,f,*]

[a]Department of Bioengineering, The University of Utah, United States

[b]Division of Clinical Biotechnology, Center for Disease Biology and Integrative Medicine, Graduate School of Medicine, The University of Tokyo, Japan

[c]Department of Otorhinolaryngology and Head and Neck Surgery, Graduate School of Medicine and Faculty of Medicine, The University of Tokyo, Japan

[d]Department of Bioengineering, Graduate School of Engineering, The University of Tokyo, Japan

[e]Department of Pharmaceutics and Pharmaceutical Chemistry, The University of Utah, United States

[f]Utah-Inha DDS and Advanced Therapeutics Research Center, Incheon, Korea

Abstract

A dose circulating through the blood at one time will have different opportunities to access the tumor compared to a dose circulating hours later. Methods to test this hypothesis allowed us to differentiate two uniquely fluorescent doses of nanoparticles (administered as a mixture or sequentially) and to measure the distribution and correlation of these nanoparticle doses in three dimensions. Multiple colocalization analyses confirm that silica nanoparticles separated into different dose administrations will not accumulate in the same location. Decreased colocalization between separate doses implies dynamic extravasation events on the scale of microns. Further, the perfusion state of different blood vessels can change across the dosing period. Lastly, analyzing the distance traveled by these silica nanoparticles in two dimensions can be an overestimation when compared with three-dimensional distance analysis. Better understanding intratumoral distribution of delivered drugs will be crucial to overcoming the various barriers to transport in solid tumors.

[*]Corresponding author: You Han Bae, PhD, Department of Pharmaceutics and Pharmaceutical Chemistry, College of Pharmacy, University of Utah, Rm 2972, Skaggs Pharmacy Institute, 30S 2000E, Salt Lake City, Utah 84112, USA, Phone: 801-585-1518, you.bae@utah.edu.

Supplementary Material Available

Supplementary material in a PowerPoint file is provided for additional figures and video. The figures show data characterizing the silica nanoparticles, the original (non-thresholded) versions of the example images shown in Figure 1, more comprehensive graphs for Mander's and Pearson's values showing the different experimental groups (varying intervals for separately dosed administrations), and an additional set of images from different time points for Figure 3B analyzing transiently overlapped and unique perfusion events. The videos are the intravital imaging data. This material is available via the Internet.

Graphical abstract

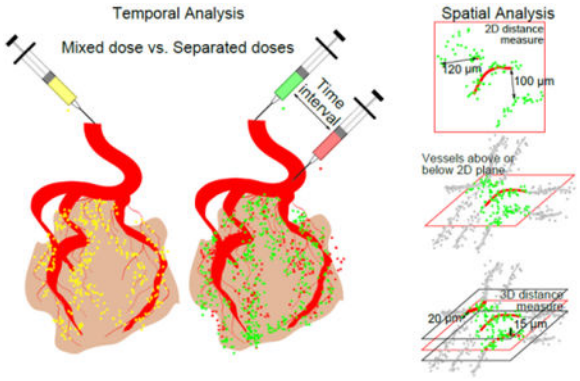

Keywords

solid tumors; nanoparticles; perfusion; extravasation; dynamic drug delivery

Introduction

In the past few decades, nanoparticles have become popular tools to make inroads into treating cancerous tumors. Traditional chemotherapy causes widespread toxicity to the entire body in order to treat the cancer. Drug delivery via nanoparticles seeks to be a magic bullet that limits toxicity to the cancer. However, nanoparticles still must rely on passive delivery mechanisms. There are numerous barriers that stand in their way of treating the tumor. They pass through the blood circulation and encounter other organs or tissues where they may become sequestered by the mononuclear phagocyte system (MPS). Even when they encounter the tumor there are still more barriers that inhibit transport and delivery.

This research focuses on understanding distribution in the intratumoral environment. Many nanoparticle based treatments rely on the enhanced permeability and retention (EPR) of macromolecules in solid tumors, but more research needs to be done to test some of the assumptions. The way to access an inoperable solid tumor is via the vasculature. Often the vasculature of the tumor does not cover the entire tumor volume evenly. That limits access to certain parts of the tumor. Studies show that solid tumors often prevent the penetration of macromolecules far beyond the proximity of blood vessels [1–3]. Furthermore, the distribution of these extravasation locations appears to be heterogeneous within the tumor environment [3]. This is likely due to the remodeling of the vascular networks in a nutrient hungry tumor with increased angiogenesis.

The details of intratumoral distribution are still uncertain. Beyond the assumptions made related to accumulation via the EPR, it is difficult to predict how the drug dose will distribute inside of the tumor environment. This research builds on research seeking to quantify drug distribution in the intratumoral environment. This research tests the hypothesis that these extravasation events are not only heterogeneous in location, but also dynamic in time. Specifically, we sought to explore how the drug distribution may change over time by differentiating an earlier dose from a later dose. Furthermore, we sought to glean additional

information by observing the distribution of the two uniquely fluorescent doses in real-time with intravital microscopy. Finally, we hypothesized that calculating the distance to nearest blood vessels would be different for two dimensions (2D) and three dimensions (3D).

As an analogy for the value of understanding accessibility changes over time, modern online maps with navigation suggestions allow us to select a day and time to see typical traffic patterns for the given conditions. It provides information on which routes are going to be blocked and which routes have access. If similar predictions for access to a tumor could be offered, this would be valuable information when delivering drug to a tumor given certain conditions. As we currently treat clinical tumors, the tumor mass can be reduced with delivered drugs; however, partially due to the limited delivery of drug to the entire tumor, the tumor will eventually resist treatment and grow back in a more aggressive state.

This research will help characterize EPR as it exists in the majority of tumors used in preclinical studies. For that reason, a xenograft mouse model is used. Perhaps by understanding EPR in this model, we might discover some flaws that explain why results do not always translate to the clinical setting.

Materials/Methods

Red and green fluorescent silica nanoparticles were purchased from micromod (40-00-701 and 42-00-701, Rostock, Germany) and their sizes and surface charges were verified with dynamic light scattering and zetapotential measurements using a Malvern Zetasizer. Athymic nude mice (Simonsen Labs, Gilroy, CA) were injected subcutaneously with a 100 μL PBS solution (20% FBS) containing HeLa cells (7.5×10^6 cells) or HT29 cells (1.25×10^6 cells) in the rear flank to initiate tumor growth. When the tumor volume reached approximately 100 mm^3, the mice would receive tail vein injections of silica nanoparticle solutions at a concentration of 20 mg/kg for each dose. The red and green silica nanoparticles were either administered as a mixed solution or separately with varying intervals, ranging from 30 minutes to 12 hours. Unless otherwise stated (two groups in SF3 and one mouse in Figure 3C), the green silica nanoparticles were injected as the first dose followed by red silica nanoparticles as the second dose. Three hours after the final dose, the mice were sacrificed and 1,1’ - Dioctadecyl - 3,3,3’,3’ - tetramethylindodicarbocyanine iodide (DiD) (84903, Anaspec, Fremont, CA) was introduced by cardiac perfusion to fluorescently stain the blood vessels. This vessel staining protocol was previously found to be adequate in staining even the small vessels of densely packed human fibroid tissue [4]. Following perfusion, the liver and tumor tissues were collected and placed in Optimal Cutting Temperature compound for at least 5 minutes before flash freezing with isopentane in a metal beaker cooled by liquid nitrogen. Samples were stored at −80°C until sectioning with a cryotome at a thickness of 100 μm for mounting on microscopy slides. As all probes and stains were introduced before harvesting tissues, no further staining was required and this also facilitated acquisition for 3D image stacks. A Nikon A1 confocal microscope with a motorized stage automated the process of acquiring 3D Z stacks and stitched mosaics of the entire tissue section. Sequential imaging was performed to isolate each fluorescent signal: green silica nanoparticles were excited at 488 nm, red silica nanoparticles at 561 nm, and the

DiD stain at 638 nm. The acquired images were then processed in batches with custom MATLAB code to determine the distribution and colocalization of the multiple doses.

Binary images were created by applying a threshold to the images. A distance map was created from the binary blood vessel image. The pixel values in the distance map gave the Euclidean distance from that pixel to the nearest blood vessel (in 2D or 3D). This distance map was multiplied by the binary image for the nanoparticle signal to assign distance values for each pixel representing nanoparticles. The code also assigned primary colors and unique values to each binary channel to facilitate qualitative observation and quantitative summation of overlapped or unique pixels.

The percent overlap provides the simplest and most intuitive measure for colocalization of the two signals by showing the overlap of detected signal objects relative to the total signal from either the first or second dose of silica nanoparticles.

$$1stDose\ \%\ overlap = \frac{\sum Rt \cap Gt}{\sum Gt} \times 100$$

$$2ndDose\ \%\ overlap\ = \frac{\sum Rt \cap Gt}{\sum Rt} \times 100$$

where Gt and Rt represent the thresholded binary values of signal coming from the green and red silica nanoparticles, respectively, for each pixel. The intravital images were only analyzed for percent overlap to simply show whether or not the signal was there and overlapping.

The end-point analysis of extravasated silica nanoparticles used Pearson's and Mander's coefficient values to look at more than just binary presence of the signal, but also at the intensity (or concentration) correlation which was present. The colocalization analysis by these means was more robust even if the signal was dim or had background noise [5,6]. These further colocalization analyses were performed by first creating a mask or region of interest based on the thresholded silica nanoparticle images. With the region of interest defined, the original, nonthresholded images were used to calculate the correlation between green and red signals. Defining a region of interest for colocalization analysis eliminated the large areas of background containing common blackness or random signal noise which could erroneously increase or decrease, respectively, the correlation value.

The Mander's value describes the fraction of overlap from the two signals' intensities.

$$Mander's = \frac{\sum_i \mathrm{R}_i \cdot \mathrm{G}_i}{\sum_i \mathrm{R}i^2 \cdot \sum_i \mathrm{G}i^2}$$

where Ri and Gi represent the intensities for red and green signal, respectively, in each pixel. The equation for Pearson's value subtracts the average value for red or green (R_{avg} or G_{avg})

and provides information on the covariance of the two signals: if the two signals tend to increase together the value is closer to 1.

$$Pearson's = \frac{\sum_i \left(\left(R_i - R_{avg}\right)\left(G_i - G_{avg}\right)\right)}{\sqrt{\sum_i (R_i - R_{avg})^2 \cdot \sum_i (G_i - G_{avg})^2}}$$

Furthermore, this subtraction allows for a value as low as −1 which indicates that one signal tends to increase while the other decreases.

Multiple areas from numerous Z stacks were analyzed for correlation between the nanoparticle signals. A p value was produced by the built in MATLAB corrcoef function to represent the chances of getting the same correlation by random chance. Only images with a p value less than 0.05 were included in the averages. The MATLAB code generated both Pearson's and Mander's values describing the colocalization of the two silica nanoparticle signals. Finally, these values were averaged for the groups of mice and statistical significance of the separately dosed mice having a lower value was calculated with a Student's t-test.

Intravital imaging was performed using a Nikon A1R confocal laser scanning microscope system attached to an upright ECLIPSE Ni-E equipped with a CFI Plan Apo Lambda 20× objective. The blood circulation half-lives of the two colors of silica nanoparticles were determined by checking the fluorescence intensity in the blood vessels of the ear-lobe of mice using the microscopy methods described in previously published work [7]. To prepare the tumor bearing mice, 6–8 w old female BALB/c nu/nu mice (Charles River Laboratories Japan, Inc., Kanagawa, Japan) were subcutaneously inoculated with murine colon carcinoma C26 cells (American Type Culture Collection, Manassas, VA, USA). Mice were anesthetized and maintained with 1.0–1.5% isoflurane onto a stage-top temperature-controlled pad calibrated at 37°C. The tumor was imaged as 6 dimensions composed of XY Large Scan (using a motorized stage), Z stack (10 μm thickness, three slices), Time-Lapse (10 min interval), and 2 Channels (green and red). Two mice were administered with green silica nanoparticles 10 minutes after the imaging was initiated. After 2 hours, the red silica nanoparticles were administered. The order was switched for one mouse as a control.

Results/Discussion

The silica nanoparticle batches of different colors were characterized and it was confirmed that both have a hydrodynamic diameter of about 73 nm, a strong negative surface charge, and halflife in the blood of about 30 minutes (SF1).

We chose simple, inorganic, fluorescent nanoparticles because the characteristics could be controlled and verified to be nearly identical. Although it is anticipated that protein adhesion and aggregation will occur upon entering the body (like any nanoparticle), degradation into smaller particles was not a concern as the in vivo experiments lasted no longer than a day and significant degradation of non-porous silica nanoparticles takes longer than a week [8,9].

Two uniquely fluorescent doses of silica nanoparticles were administered either as a mixed dose or separately at varying intervals for temporal analysis. When the two uniquely fluorescent silica nanoparticles are administered separately, the two colors can be distinguished with some non-overlapping signal. Figure 1 shows qualitative and quantitative differences in colocalization between mixed and separate doses for representative images in liver and tumor tissue.

The two fluorescent signals were analyzed for colocalization in the tumor environment and compared with values from the liver as a positive control. The liver was chosen as it has more reliable silica nanoparticle accumulation and a better signal/noise ratio. The better signal to noise ratio, the more consistent the correlation was. This accumulation in the liver is characteristic of hepatic circulation from tail vein administration [10]. Notoriously leaky vessels in the sinusoids allow for high accumulation of nanoparticles and the Kupffer cells in the liver could phagocytose the nanoparticles into concentrated, bright bundles. As a comparison for showing dynamic events, the phagocytosis is clearly not a static event and the dynamic leakiness of liver sinusoids has been summarized in a review article [11]. When the two doses were mixed together and then administered, there was a high percentage of signal overlap in both the tumor and liver tissue. However, the lower percentages of signal overlap for separately administered doses suggest dynamics in both the liver and tumor environments.

The overlap analysis in Figure 2A merely shows a trend supporting the hypothesis that separate doses will have decreased colocalization. Unlike Figure 1, the data in Figure 2 only includes images of tumor tissue where the signal was weaker and not as consistent. Simple overlap analysis is not as robust for the weak nanoparticle signal outside of the blood vessel in the tumor tissue where there is also more background noise. A noteworthy difference is that the 2^{nd} dose signal had a better signal to noise ratio and the data was significant. In contrast, the 1^{st} dose appeared more diffuse and weak. Quantifying the colocalization with additional, more sophisticated, colocalization techniques found a statistical difference when comparing the Pearson's and Mander's values for mixed and separate doses in the tumor (Figure 2B).

Correlation analysis for various dosing intervals sought to identify a spectrum of temporal dynamics in the tumor environment. Unfortunately, we were not able to discern significant differences between the various dosing intervals, but merely the difference between mixed and separate doses. The analysis may result in false negatives for dynamic extravasation or false positives for colocalization (it is unable to resolve two different nanoparticles that are spaced only 100 nm apart). The point spread function for the Nikon A1 microscope used for these experiments gives a theoretical resolution of 147 nm along the X and Y axis and 368 nm along the Z axis in ideal conditions. Furthermore, the 3D image acquisition with certain step sizes effectively set the resolution as low as 5 μm along the Z axis. Other processing techniques, such as thresholding for distance or object overlap analysis, further reduced the resolution. Explorative calculations based on regions of interest determined by thresholds generally only varied by 10 μm. Thus, the figures of merit for this approach put our resolution near 5 to 10 μm. This allows for detection of dynamic extravasation events from blood vessels (as a result of remodeling) that are at least 50 μm (length of endothelial cell)

apart from each other. Thus, we could still determine whether dynamic extravasation events occurred in intratumoral drug delivery. To observe dynamics on a larger scale, intravital microscopy was performed with a purpose of verifying and teasing out additional results.

Real-time intravital microscopy showed strong signals for the fluorescent nanoparticles in the blood vessels (Figure 3). Analysis of the fluorescent signals through the perfused vessels suggests dynamics in entire blood vessels within the tumors. Overlap analysis demonstrates that a dose can have as much as 98% or as little as 34% of its perfusion overlapped with the other dose. Some vessels maintained high signal levels for both doses and showed high overlap. Other vessels showed strong signals, only to fade with blood clearance of the nanoparticles. Finally, some vessels appeared to only show signal for one of the two doses (often the first dose). Averaging the 3 mice, the first dose had more unique signal locations and the second dose had a higher percentage of signal overlap. Image C of Figure 3 appears to be an exception to this, but further inspection reveals that the two doses perfuse through many of the same vessels (Figure 4). Due to the blood circulation half-life being shorter than the administration interval, the overlap of signal in these vessels were low. This implies that the majority of dynamics (on this time scale) results in blood vessels closing off and preventing access for the second dose. The trend of high overlap for the second dose was not observed in the end-point analysis of extravasation into the tumor tissue. In that case, the second dose can continue to have low overlap due to dynamic extravasation events beyond dynamic perfusion events. Dynamic extravasation and perfusion events are each on a different spatial scale which greatly affects determination of colocalization.

The spatial analysis (presented qualitatively and quantitatively in Figure 5) found that measuring the distance of extravasated nanoparticles from the blood vessel in only 2D often overestimates the distance traveled. This can be seen qualitatively when comparing the 2D and 3D distance maps. The 3D distance map shows a similar pattern for all slices of the Z stack because blood vessels in one slice influence the distance map in slices above or below. For our collection of images, we found that the average overestimation of distance traveled by 2D measurements compared to 3D was about 25 μm. The distance measurements in 2D had a large spread of values when comparing the different Z stacks of a given tissue volume. If investigators were to analyze a 2D slice from region 4 in Figure 5C, there is the potential to overestimate the distance by about 150 μm in that case. Three regions of negative control result in very low distances as would be expected when no nanoparticles are administered, but one had some speckles of background noise or non-specific staining that was included in the distance analysis. Other regions had low distance values simply because some tumor regions had stronger signal from silica nanoparticles than others.

The overestimation in distance traveled occurs as most 2D methods cannot include any possible vessels above or below the frame of interest. However, even with imaging tissue sections in 3D, there is still the chance for slight overestimation of distance traveled as there may be a vessel just beyond the tissue section being imaged. It is possible to image all sections of the entire tumor; however, the increase in accuracy is likely not proportional to the increase in required resources. Similarly, some meaningful trends can still be observed with 2D distance analysis. Still, given the ease of obtaining 3D stacks with confocal

microscopes, we recommend distance measurements be performed in 3D when possible for increased accuracy.

Calculating distance between vessel and nanoparticle objects identified by thresholding relies heavily on the threshold value chosen. Thresholding can shift the mean distance from the nearest blood vessel, but two things will remain: the 2D distance measurement will be greater than the 3D measurement and the 2D measurement will have greater variability. Finally, it is possible that the DiD stain introduced via cardiac perfusion may not stain all blood vessels. The high interstitial fluid pressure may cause some blood vessels to collapse or have limited perfusion. We chose to measure distances from perfused vessels because we were not interested in measuring distances from occluded vessels, from which the particles likely did not extravasate from. With our results confirming dynamic perfusion of blood vessels, it becomes more challenging to know from which blood vessels you should measure the distance traveled.

Researchers are looking into the effect of size and shape on extravasation and penetration into the tumor environment [12–14]. Generally, the smaller particles have higher permeability and diffuse more rapidly in tumors [15]. Future experiments could investigate whether different sizes could be susceptible to different extravasation events (from the cellular level with fenestrae and intercellular gaps to larger events resulting in blood lakes or when vessels change their perfusion state) and thus be sensitive to different dynamics relating to colocalization [16]. Analyzing different sizes is also relatable to determining how aggregated particles are influenced by the dynamics. We have already built computer models to understand how extravasation events occur [17]. We will continue to develop these and other numerical models to test various parameters. Future experiments will also need to test the effects of pro or antiangiogenic factors on the dynamic leakiness of these tumor blood vessels. These experiments should determine the cause of the dynamics at the different levels and whether the multiple doses have a direct effect on each other via saturation or blocking effects. It is possible that vessels could become embolized from aggregated nanoparticles and new perfusion events could occur from sprouting vessels. On the other hand, solid stress inside the tumor could play a role in the opening and closing of vessels. It is known that tumors can cause lymph and blood vessels to collapse, but treatments can reverse this and increase the number of patent vessels [18,19]. Even without therapeutic intervention, Debbage *et al.* previously showed dynamic perfusion using lectin stains [20]. The results herein confirm that phenomenon using fluorescent nanoparticles in the blood circulation. We further showed how dynamics influence the extravasation of the doses to different locations in the interstitial space. Understanding these dynamics will educate how access to the tumor via the vasculature can be in an open or closed state.

Knowing how access to the tumor may change over time may influence planning of dosing schedules and combinatorial strategies in the clinical setting. With a lower fraction of unique perfusion for the second dose 2 hours after the first, long circulation may not be beneficial in all aspects. A relevant clinical trial showed that filtering liposomal doxorubicin 24 hours after administration reduced side effects yet did not discern a change in efficacy [21]. The authors speculate that the tumor tissue had become saturated and all other drug particles circulating were likely to cause toxicity in healthy tissue. This is backed up by the fact that

the non-PEGylated version of Doxil (Myocet) has a lower occurrence of palmar plantar erythrodysesthesia syndrome [22,23]. Clinical dosing schedules are often around 2 weeks apart. The dosing schedule is primary limited by the toxicity of treatment, but this is much longer than the half-life of the drugs administered. Thus, each dosing may have different access to the tumor. Many first line cancer therapies involve combinations of drugs to improve efficacy and limit resistance. The efficacy of concurrent versus sequential administrations have been studied in cells, xenografts in mice, and even in patients. Though not conclusive, concurrent therapy tends to be more favorable than sequential [24–28]. In addition to cell cycles, dynamics in vascular access may be a contributing factor in these studies. Concurrent therapy is more likely to deliver the combinatorial drugs to the same location in the tumor and allow synergistic benefits. Newer drug carrier formulations are considering whether it is better to combine two drugs into one carrier as opposed to having each drug in separate carriers [29]. Some clinicians may prefer the control afforded by having each drug in separate carriers. This would allow different release rates for each carrier and the ability to modify drug ratios by adjusting the carrier weight ratios. However, until more details on dynamic extravasation events over time and dynamic perfusion events of vessel segments within the tumor can be elucidated, a single carrier housing both drugs best ensures they reach the same locations (at the ratios intended) in the tumor.

Conclusion

While dynamic perfusion and extravasation events have been shown in animal tumors that grow faster with chaotic vasculature, similar experiments need to probe clinical tumors for similar dynamics. Targeting the tumor environment through EPR is passive delivery and relying on passive delivery in the complex tumor environment appears to be inconsistent—especially in clinical applications [30]. Perhaps nanoparticles characteristics can be tuned to provide a way to mitigate the dynamic events observed in the chaotic tumor environment. Alternatively, methods of altering the tumor environment (via the vasculature or other contributors to pressure) may prove to be necessary to return the tumor environment to a more predictable and consistent state for delivering multiple doses.

Supplementary Material

Refer to Web version on PubMed Central for supplementary material.

Acknowledgments

End-point microscopy imaging was performed at the University of Utah’s Fluorescence Microscopy Core Facility, a part of the Health Sciences Cores at the University of Utah. Microscopy equipment was obtained using a NCRR Shared Equipment Grant # 1S10RR024761-01. The project was also supported with grants from the National Institutes of Health: CA101850 and CA122356.

Intravital microscopy imaging was performed at the University of Tokyo. The equipment was obtained and supported using the CREST and COI Program from Japan Science and Technology, the FIRST Program from the Japan Society for the Promotion of Science, and KAKENHI Grant Numbers 2379004 (YM), 15K06871 (KT), and 25000006 (KK) from the Japanese Ministry of Education, Culture, Sports, Science and Technology.

References

[1]. Dreher MR, Liu W, Michelich CR, Dewhirst MW, Yuan F, Chilkoti A, Tumor Vascular Permeability, Accumulation, and Penetration of Macromolecular Drug Carriers, J. Natl. Cancer Inst 98 (2006) 335–344. [PubMed: 16507830]

[2]. Primeau AJ, Rendon A, Hedley D, Lilge L, Tannock IF, The distribution of the anticancer drug Doxorubicin in relation to blood vessels in solid tumors., Clin. Cancer Res 11 (2005) 8782–8. doi:10.1158/1078-0432.CCR-05-1664. [PubMed: 16361566]

[3]. Yuan F, Leunig M, Huang SK, Berk DA, Papahadjopoulos D, Jain RK, Microvascular Permeability and Interstitial Penetration of Sterically Stabilized (Stealth) Liposomes in a Human Tumor Xenograft, Cancer Res. 54 (1994) 3352–3356. [PubMed: 8012948]

[4]. Stirland DL, Nichols JW, Jarboe E, Adelman M, Dassel M, Janát-Amsbury M-M, et al., Uterine perfusion model for analyzing barriers to transport in fibroids., J. Control. Release 214 (2015) 85–93. doi:10.1016/j.jconrel.2015.07.006. [PubMed: 26184049]

[5]. Dunn KW, Kamocka MM, McDonald JH, A practical guide to evaluating colocalization in biological microscopy, AJP Cell Physiol. 300 (2011) C723–C742. doi:10.1152/ajpcell.00462.2010.

[6]. Manders EMM, Verbeek FJ, Aten JA, Measurement of co-localization of objects in dual-colour confocal images, J. Microsc 169 (1993) 375–382. doi:10.1111/j.13652818.1993.tb03313.x.

[7]. Nomoto T, Matsumoto Y, Miyata K, Oba M, Fukushima S, Nishiyama N, et al., In situ quantitative monitoring of polyplexes and polyplex micelles in the blood circulation using intravital real-time confocal laser scanning microscopy, J. Control. Release 151 (2011) 104–109. doi:10.1016/j.jconrel.2011.02.011. [PubMed: 21376766]

[8]. Yamada H, Urata C, Aoyama Y, Osada S, Yamauchi Y, Kuroda K, Preparation of Colloidal Mesoporous Silica Nanoparticles with Different Diameters and Their Unique Degradation Behavior in Static Aqueous Systems, Chem. Mater 24 (2012) 1462–1471. doi:10.1021/cm3001688.

[9]. Park J-H, Gu L, von Maltzahn G, Ruoslahti E, Bhatia SN, Sailor MJ, Biodegradable luminescent porous silicon nanoparticles for in vivo applications., Nat. Mater 8 (2009) 331–6. doi:10.1038/nmat2398. [PubMed: 19234444]

[10]. Yildirimer L, Thanh NTK, Loizidou M, Seifalian AM, Toxicology and clinical potential of nanoparticles., Nano Today. 6 (2011) 585–607. doi:10.1016/j.nantod.2011.10.001. [PubMed: 23293661]

[11]. Braet F, Wisse E, Structural and functional aspects of liver sinusoidal endothelial cell fenestrae: a review., Comp. Hepatol 1 (2002) 1 http://www.pubmedcentral.nih.gov/articlerender.fcgi?artid=131011&tool=pmcentrez&rendertype=abstract (accessed October 30, 2013). [PubMed: 12437787]

[12]. Smith BR, Kempen P, Bouley D, Xu A, Liu Z, Melosh N, et al., Shape matters: intravital microscopy reveals surprising geometrical dependence for nanoparticles in tumor models of extravasation., Nano Lett. 12 (2012) 3369–77. 10.1021/nl204175t (accessed August 16, 2012). [PubMed: 22650417]

[13]. Cabral H, Matsumoto Y, Mizuno K, Chen Q, Murakami M, Kimura M, et al., Accumulation of sub-100 nm polymeric micelles in poorly permeable tumours depends on size., Nat. Nanotechnol 6 (2011) 815–23. doi:10.1038/nnano.2011.166. [PubMed: 22020122]

[14]. Perrault SD, Walkey C, Jennings T, Fischer HC, Chan WCW, Mediating tumor targeting efficiency of nanoparticles through design., Nano Lett. 9 (2009) 1909–15. doi:10.1021/nl900031y. [PubMed: 19344179]

[15]. Jain RK, Stylianopoulos T, Delivering nanomedicine to solid tumors., Nat. Rev. Clin. Oncol 7 (2010) 653–64. doi:10.1038/nrclinonc.2010.139. [PubMed: 20838415]

[16]. Hashizume H, Baluk P, Morikawa S, McLean JW, Thurston G, Roberge S, et al., Openings between Defective Endothelial Cells Explain Tumor Vessel Leakiness, Am. J. Pathol 156 (2000) 1363–1380. [PubMed: 10751361]

[17]. Matsumoto Y, Nichols J, Toh K, Nomoto T, Cabral H, Miura Y, et al., Vascular bursts enhance permeability of tumour blood vessels and improve nanoparticle delivery., Nat. Nanotechnol (in press). doi:10.1038/nnano.2015.342.

[18]. Padera TP, Stoll BR, Tooredman JB, Capen D, di Tomaso E, Jain RK, Pathology: Cancer cells compress intratumour vessels, Nat. Commun 427 (2004) 695.

[19]. Chauhan VP, Martin JD, Liu H, Lacorre DA, Jain SR, V Kozin S, et al., Angiotensin inhibition enhances drug delivery and potentiates chemotherapy by decompressing tumour blood vessels., Nat. Commun 4 (2013) 2516. doi:10.1038/ncomms3516. [PubMed: 24084631]

[20]. Debbage PL, Griebel J, Ried M, Gneiting T, DeVries A, Hutzler P, Lectin Intravital Perfusion Studies in Tumor-bearing Mice: Micrometer-resolution, Wide-area Mapping of Microvascular Labeling, Distinguishing Efficiently and Inefficiently Perfused Microregions in the Tumor, J. Histochem. Cytochem 46 (1998) 627–639. doi:10.1177/002215549804600508. [PubMed: 9562571]

[21]. Eckes J, Schmah O, Siebers JW, Groh U, Zschiedrich S, Rautenberg B, et al., Kinetic targeting of pegylated liposomal doxorubicin: a new approach to reduce toxicity during chemotherapy (CARL-trial)., BMC Cancer. 11 (2011) 337 http://www.biomedcentral.com/1471-2407/11/337 (accessed August 10, 2012). [PubMed: 21816044]

[22]. Swenson CE, Bolcsak LE, Batist G, Guthrie THJ, Tkaczuk KH, Boxenbaum H, et al., Pharmacokinetics of doxorubicin administered i.v. as Myocet (TLC D-99; liposomeencapsulated doxorubicin citrate) compared with conventional doxorubicin when given in combination with cyclophosphamide in patients with metastatic breast cancer, Anticancer. Drugs 14 (2003). http://journals.lww.com/anticancerdrugs/Fulltext/2003/03000/Pharmacokinetics_of_doxorubicin_administered_i_v_.8.aspx.

[23]. Batist G, Cardiac safety of liposomal anthracyclines., Cardiovasc. Toxicol 7 (2007) 72–4. doi:10.1007/s12012-007-0014-4. [PubMed: 17652807]

[24]. Cavalli F, Beer M, Martz G, Jungi WF, Alberto P, Obrecht JP, et al., Concurrent or sequential use of cytotoxic chemotherapy and hormone treatment in advanced breast cancer: report of the Swiss Group for Clinical Cancer Research., BMJ. 286 (1983) 5–8. doi:10.1136/bmj.286.6358.5. [PubMed: 6401458]

[25]. Francis P, Crown J, Di Leo A, Buyse M, Balil A, Andersson M, et al., Adjuvant chemotherapy with sequential or concurrent anthracycline and docetaxel: Breast International Group 02–98 randomized trial., J. Natl. Cancer Inst 100 (2008) 121–33. doi:10.1093/jnci/djm287. [PubMed: 18182617]

[26]. Fung AS, Wu L, Tannock IF, Concurrent and sequential administration of chemotherapy and the Mammalian target of rapamycin inhibitor temsirolimus in human cancer cells and xenografts., Clin. Cancer Res 15 (2009) 5389–95. doi:10.1158/10780432.CCR-08-3007. [PubMed: 19706800]

[27]. Citron ML, Berry DA, Cirrincione C, Hudis C, Winer EP, Gradishar WJ, et al., Randomized trial of dose-dense versus conventionally scheduled and sequential versus concurrent combination chemotherapy as postoperative adjuvant treatment of nodepositive primary breast cancer: first report of Intergroup Trial C9741/Cancer and Leukemia, J. Clin. Oncol 21 (2003) 1431–9. doi:10.1200/JCO.2003.09.081. [PubMed: 12668651]

[28]. Fournel P, Robinet G, Thomas P, Souquet P-J, Léna H, Vergnenégre A, et al., Randomized phase III trial of sequential chemoradiotherapy compared with concurrent chemoradiotherapy in locally advanced non-small-cell lung cancer: Groupe Lyon-SaintEtienne d'Oncologie Thoracique-Groupe Français de Pneumo-Cancérologie NPC 95–01 Study., J. Clin. Oncol 23 (2005) 5910–7. doi:10.1200/JCO.2005.03.070. [PubMed: 16087956]

[29]. Bae Y, Diezi TA, Zhao A, Kwon GS, Mixed polymeric micelles for combination cancer chemotherapy through the concurrent delivery of multiple chemotherapeutic agents., J. Control. Release 122 (2007) 324–30. doi:10.1016/j.jconrel.2007.05.038. [PubMed: 17669540]

[30]. Stirland DL, Nichols JW, Miura S, Bae YH, Mind the gap: A survey of how cancer drug carriers are susceptible to the gap between research and practice, J. Control. Release 172 (2013) 1045–1064. [PubMed: 24096014]

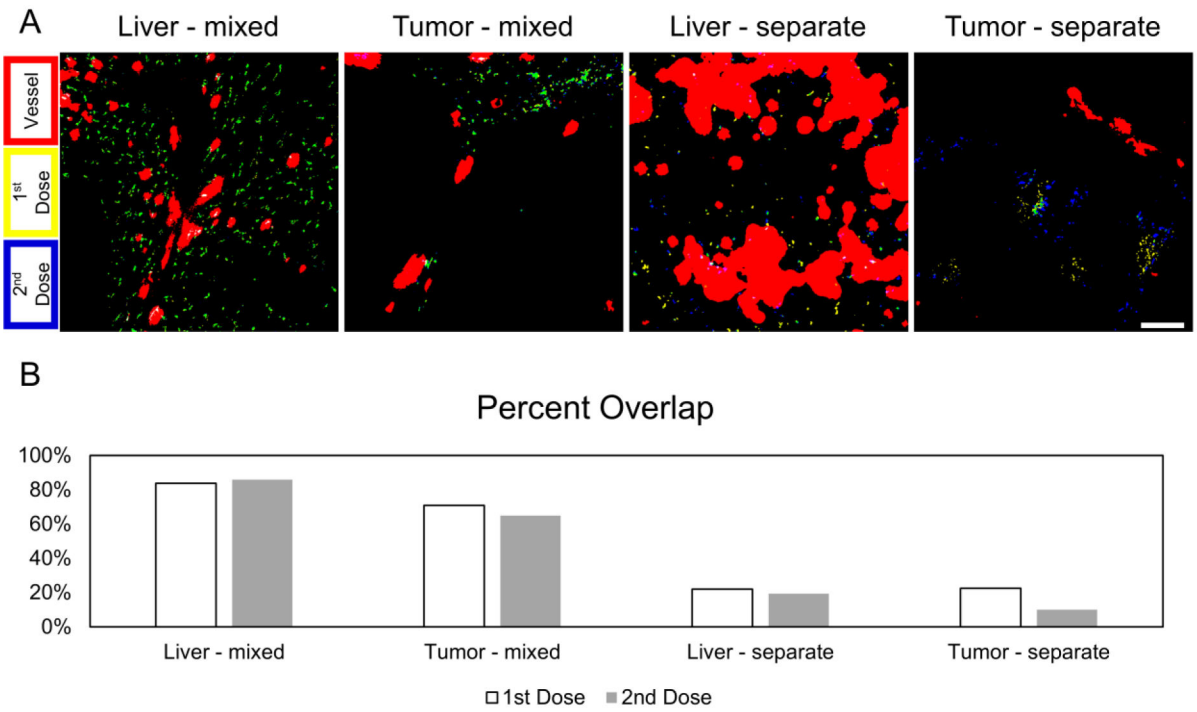

Figure 1.

Representative images of the fluorescent signals from two silica nanoparticle doses in liver and tumor tissues. A) The example images are thresholded to show high-contrast images of the signals for blood vessel (red), 1st dose (yellow), and 2nd dose (blue). Furthermore, secondary colors represent overlapping signal (e.g., green for overlap of the two dose signals). Scale bar is 100 μm and applies to all images. B) The example images were quantified for the percent overlap of each dose.

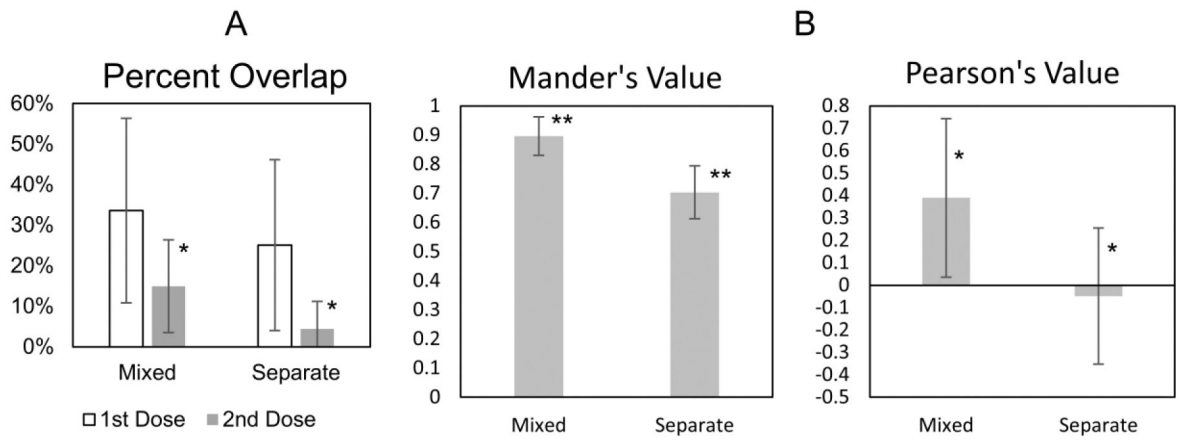

Figure 2.

Colocalization analysis of silica nanoparticle doses in tumor tissues. Error bars are standard deviation. * $p < 0.05$. ** $p < 0.01$. A) Average values for percent overlap analysis for a larger data set of 10 different mice: 4 with mixed doses and 6 with separate doses. B) Average Mander's and Pearson's values for 24 different mice: 4 with a mixed dose and 20 separately dosed.

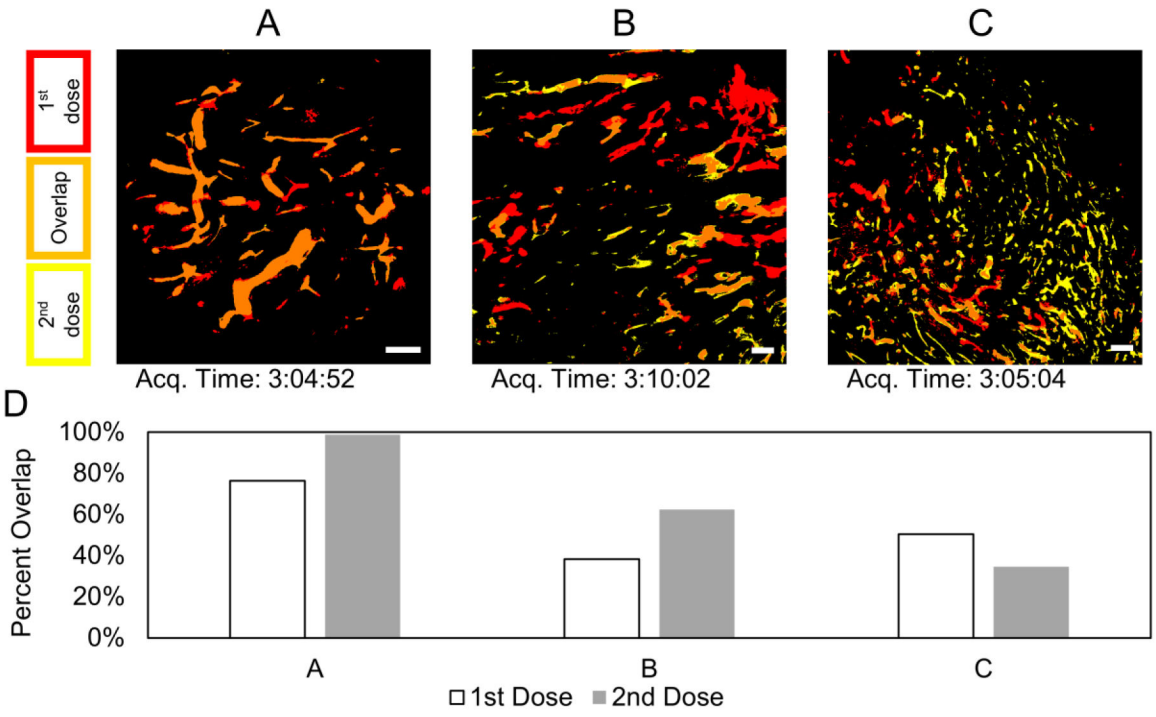

Figure 3.

Thresholded images from intravital microscopy for three different mice (A, B, C) showing blood vessels perfused with silica nanoparticles. For (A and B), the green silica nanoparticles were administered first; then after 2 hours, the red silica nanoparticles were administered. The order of administration was reversed for (C). Scale bars are each 200 μm. D) Overlap analysis of the respective images.

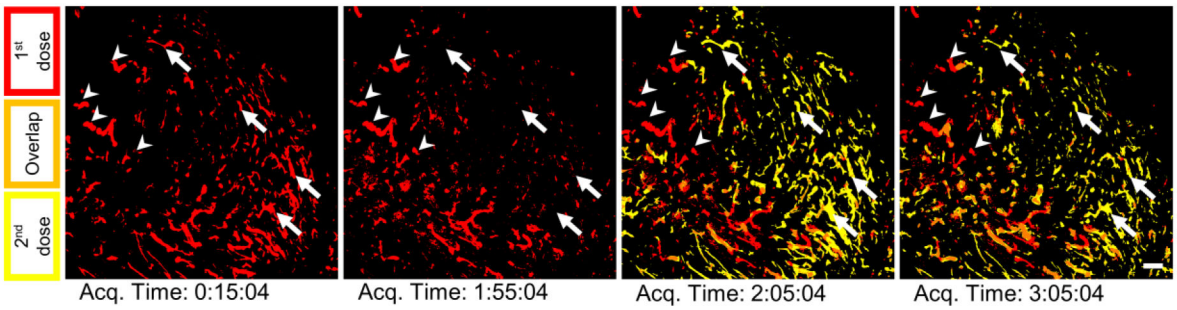

Figure 4.

Additional images for Figure 3C: right after the first dose, right before and after the second dose, and near the end of the perfusion period. Some regions (a selection marked with arrows) appear to be unique perfusion events, but instead they are just transient perfusion events for both doses such that there is little to no overlap at a given time. In other words, the areas designated by the arrows are reached by both doses but not at the same time. Other areas (a selection marked with arrowheads) appear to be only accessed by a single dose for the entire perfusion period. Scale bar is 200 μm.

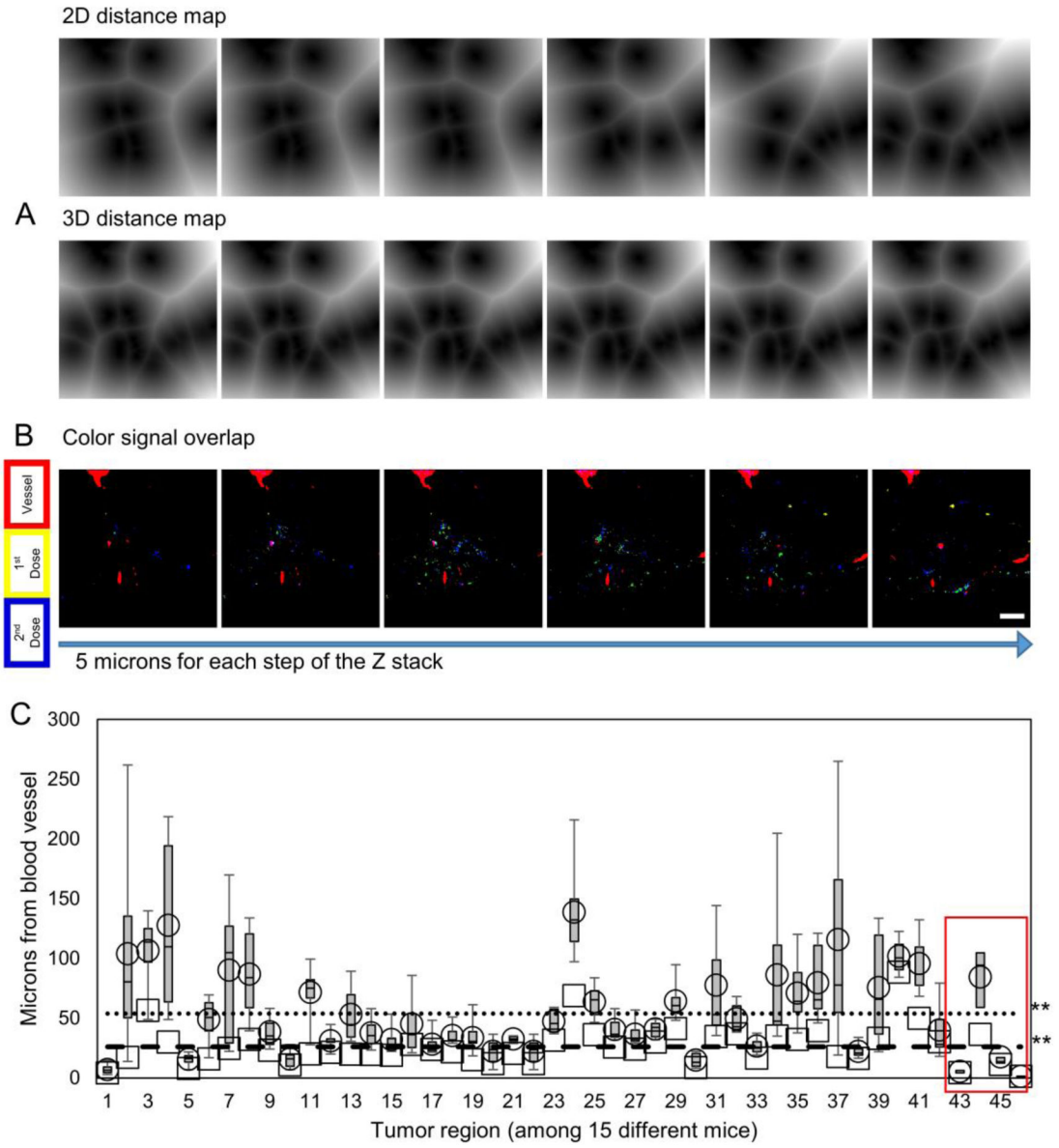

Figure 5.

Overestimation of distance traveled by 2D measurements. A) Comparison of MATLAB generated distance maps for 2D and 3D analysis. Increased brightness signifies increased distance from the blood vessel. B) Image slices are thresholded to show highcontrast images of the signals for blood vessel (red), 1st dose (yellow), and 2nd dose (blue). Secondary colors represent overlapping signal. Scale bar is 100 μm and applies to all images. C) Selection of different tumor regions (and different mice) showing how the distance traveled is overestimated when measuring in 2D versus 3D. The box plots represent the spread of 2D distance values for each tumor region. Clearly, there can be multiple 2D distance values (one for each 2D image slice through the volume of each tumor region). The open circles represent the average of all the 2D distance values for each region. The open squares represent the 3D distance values for each region. The dotted and dashed line represent the

average 2D and 3D, respectively, distance value for all the different tumor regions. The red rectangle encloses the data points from negative controls. ** $p < 0.01$.